

Robust Transit Fitting and Host-Star Modeling of 100 Transiting Exoplanet Systems

XIMING XU  ¹

¹*Department of Physics and Astronomy, University College London, London WC1E 6BT, UK*

ABSTRACT

The transit light curves of exoplanets encode not only planetary properties but also the stellar density of their host stars, providing an additional reliable constraint for stellar modeling. In this study, we applied a Bayesian inference framework to perform transit fitting and stellar modeling for 100 single-star, single-planet transiting systems with known circular orbits. The photometric data were obtained from NASA’s Transiting Exoplanet Survey Satellite (TESS). For the transit fitting, we present results for the planet-to-star radius ratio, impact parameter, and stellar density. For the majority of systems, the planet-to-star radius ratio and stellar density have mean absolute relative residuals of 3.0% and 14.4%, respectively, compared to previously published values. For the stellar modeling, we present robust estimates of stellar mass, radius, and age. In the model combining transit-derived stellar densities with spectroscopic parameters, the mean relative uncertainties (68% credible interval) are 4.1%, 3.2%, and 28.9%, respectively. This methodology can be extended to multi-planet transiting systems and to systems with non-circular orbits in future applications.

Keywords: Exoplanets (498) — Transits (1711) — Stellar properties (1624) — Bayesian statistics (1900)

1. INTRODUCTION

In 1995, the first exoplanet orbiting a main-sequence star, 51 Pegasi b, was discovered (M. Mayor & D. Queloz 1995). Over the past three decades, the field of exoplanet research has made remarkable progress. As of September 2025, 5,989 exoplanets have been confirmed, with more than 70% detected via the transit method (NASA Exoplanet Archive 2020). However, the light curves of transiting exoplanets encode not only the properties of the plan-

ets themselves, but also information about their host stars, the stellar density (ρ_*) (S. Seager & G. Mallen-Ornelas 2003).

Prior to the launch of the Kepler space telescope (W. J. Borucki et al. 2010), exoplanets had not yet been widely discovered via the transit method. Stellar modeling inputs primarily relied on parameters derived from spectroscopic analysis of the host stars, such as effective temperature (T_{eff}), metallicity ([Fe/H]), and surface gravity ($\log g$) (G. Takeda et al. 2007). These parameters are often strongly correlated due to degeneracies, and their ability to constrain stellar physical properties is highly model-dependent (G. Torres et al. 2012). In

Corresponding author: Ximing Xu
ucapxxu@ucl.ac.uk

Email: ucapxxu@ucl.ac.uk

contrast, the stellar density obtained from fitting transit light curves provides an additional and reliable constraint that can improve the precision of stellar modeling and deepen our understanding of the physical properties of transiting exoplanet host stars (E. Sandford & D. Kipping 2017). Following the launch of Kepler and NASA’s Transiting Exoplanet Survey Satellite (TESS) (G. R. Ricker et al. 2014), the rapid increase in the number of known transiting exoplanets has created unprecedented opportunities to improve our understanding of their host stars. Furthermore, with the growing availability of high-quality photometric data, re-analyzing known systems to refine planetary parameters and stellar densities remains both valuable and essential.

In this study, we developed a Python-based pipeline to analyze 100 transiting exoplanets and their host stars. The first stage performs transit light curve fitting using TESS photometry, using Bayesian inference implemented via nested sampling to constrain planetary parameters and stellar density. The second stage conducts Bayesian stellar modeling with a pre-computed evolutionary model grid. This two-step approach provides a consistent framework for estimating fundamental stellar properties and enhancing our understanding of host stars.

The paper is organized into the following sections. The selection and classification of the sample are described in Section 2. The methods used for transit fitting and stellar modeling are presented in Section 3. The results of the transit fitting and stellar modeling are shown in Section 4. Discussion and Conclusion are provided in Sections 5 and 6, respectively.

2. DATA AND SAMPLE

The currently known exoplanet systems exhibit considerable diversity: some host binary or multiple stars, some contain multiple planets, and some feature highly eccentric planetary orbits (NASA Exoplanet Archive 2020). Each of

these scenarios introduces additional complexity to light curve modeling. In this study, we chose to avoid such complications by selecting a sample that excludes these complex configurations. For example, assuming a circular orbit eliminates the need to fit for eccentricity or consider the planet’s position along its orbit, while focusing on single-planet systems avoids potential interference between overlapping transit signals from multiple planets.

The exoplanet sample selection in this study was based on the following criteria: (1) the planet was discovered via the transit method; (2) the planet is known to have a circular orbit; (3) the system consists of a single planet orbiting a single star; and (4) the system must have photometric observations from at least one TESS sector. To enable stellar modeling, the host star must have reported values for the following parameters: galactic coordinates, parallax, Gaia magnitude, effective temperature, and metallicity. The specific use of these parameters is described in Section 3. Furthermore, to provide a reference for the stellar density derived from transit fitting in this study, previously reported stellar density values are adopted when available. If not available, the stellar density is estimated using the reported stellar mass and radius.

Among the systems that met all of the above criteria, this study selected 100 exoplanet systems as the final sample. However, even with these simplifications, the subsequent analysis is not necessarily straightforward. In particular, light curve fitting can still be influenced by variations in transit shape and depth. As shown in Figure 1, we classified the sample into three groups based on the morphology of their light curves.

The first group represents the most ideal scenario for the transit method and is thus referred to as the ‘ideal’ group. These light curves are U-shaped, with clearly visible and deeper transit signals, which generally makes them easier

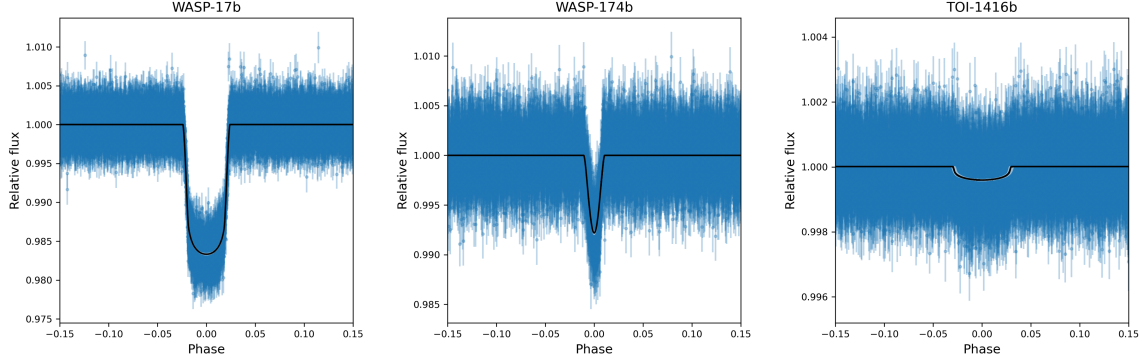


Figure 1. The three panels (from left to right) show the phase-folded light curves with the corresponding black curves indicating the best-fit transit models for WASP-17b (from the ‘ideal’ group), WASP-174b (from the ‘V-shaped’ group), and TOI-1416b (from the ‘small radius ratio’ group).

to fit. The second group is referred to as the “V-shaped” group. In some cases, the classification can be made visually—for example, the light curve of WASP-174b (Figure 1) exhibits a distinct V-shape. However, a more rigorous classification is based on a quantitative criterion involving the relationship between the impact parameter and the planet-to-star radius ratio, as defined in Equation 1. Systems that satisfy the conditions for a grazing transit are assigned to this group.

$$\text{case} = \begin{cases} \text{full transit, for } 0 \leq b \leq 1 - \frac{R_p}{R_*} \\ \text{grazing transit, for } 1 - \frac{R_p}{R_*} < b \leq 1 + \frac{R_p}{R_*} \\ \text{no transit, for } 1 + \frac{R_p}{R_*} < b \end{cases} \quad (1)$$

The third group is referred to as the “small radius ratio” group. The transit signals in this group are relatively shallow, and due to the low signal-to-noise ratio, they can be difficult to distinguish by eye. In this study, as all photometric data were obtained from TESS to ensure data source homogeneity, samples with a transit depth (δ) less than 0.25% were classified into this category, with the threshold selected empirically for the purposes of this work. Based on Equation 2, this corresponds to a planet-to-star radius ratio ($\frac{R_p}{R_*}$) of 0.05.

$$\delta = \left(\frac{R_p}{R_*}\right)^2 \quad (2)$$

In this study, we express transit signals in terms of the planet-to-star radius ratio. However, as many previous studies report transit depth directly, careful attention must be paid to the conversion between these two quantities, particularly with respect to uncertainty propagation. Letting $y = \frac{R_p}{R_*}$ and $x = \delta$, where x is the fractional form of the transit depth, we apply the uncertainty propagation formula to derive the relationship shown in Equation 3, which describes the uncertainty in the derived radius ratio.

$$\sigma_y = \frac{1}{2\sqrt{x}}\sigma_x \quad (3)$$

At the stellar modeling stage, this study used stellar parameters available from the NASA Exoplanet Archive ([NASA Exoplanet Archive 2024](#)) as part of the input, including effective temperature and metallicity. However, values reported by different studies can vary significantly. In this analysis, we prioritized the default values listed in the dataset; if these were unavailable, we selected values from the most recent studies that provided both parameters. For stellar magnitudes, Gaia data ([T. Prusti et al. 2016](#)) were adopted for all samples to ensure consistency and homogeneity in the source of brightness measurements.

Table 1. Fitted Parameters and Prior Definitions for Transit Modeling

	Period	Epoch time	Joint Sampler (b, δ)	Stellar density
Distribution	normal	normal	uniform	loguniform
Hyperparameters	(case specific, 0.1)	(case specific, 0.1)	(0, 1)	(100, 15000)
<hr/>				
Limb-darkening coefficients	Dilution factor	Offset relative flux	Jitter term	
uniform	fixed	normal	loguniform	
(0, 1)	1	(0, 0.1)	(0.1 1000)	

NOTE—The stellar density values used in the `juliet` fitting are in SI units (kg/m^3).

3. METHODS

In this study, we developed a Python-based pipeline to perform transit light curve fitting and stellar modeling within a Bayesian inference framework. The workflow consists of three main steps: (1) extraction and preparation of TESS light curves using `lightkurve` (Lightkurve Collaboration et al. 2018); (2) transit model fitting via `juliet` (N. Espinoza et al. 2019), employing Bayesian inference with nested sampling (J. S. Speagle 2020); and (3) stellar modeling with `BASTA` (V. Silva Aguirre et al. 2015; V. Aguirre Børnsen-Koch et al. 2021) using Bayesian isochrone fitting. The complete pipeline, along with example analyses, is available in our GitHub repository². Each component is described in detail below.

3.1. *Transit Fitting*

We used `lightkurve` to extract calibrated TESS light curves produced by the Science Processing Operations Center (SPOC) at NASA Ames Research Center (J. M. Jenkins et al. 2016). These data were accessed via the Mikulski Archive for Space Telescopes (MAST). To ensure data homogeneity, we restricted our

analysis to observations with a cadence of 120 seconds.

To maximize the available data for each target, we combined all eligible TESS observations obtained up to July 2024. For each object, we generated a periodogram using the Box-Least Squares (BLS) algorithm implemented in `lightkurve` to detect and characterize periodic transit signals in the time-series data. From the resulting periodogram, we estimated the orbital period, transit duration, and epoch time. Using these parameters, we constructed a transit mask to exclude in-transit data points and ensure that the detrending process, performed with the Savitzky–Golay filter (A. Savitzky & M. J. E. Golay 1964) implemented in `lightkurve`, was not biased by transit features. The light curves were then normalized and cleaned by removing outliers and NaN values.

Using the light curves prepared with `lightkurve`, we performed transit modeling with `juliet`, which uses nested sampling via the `dynesty` sampler (J. S. Speagle 2020) to implement Bayesian inference. To obtain posterior distributions of the model parameters, appropriate prior distributions were required. The fitted parameters, along with the distributions used to define their priors and the corresponding hyperparameter values, are listed in Table 1.

² <https://github.com/XimingXu/transit-fitting-stellar-parameters>

Table 2. Input Parameters for Different Stellar Models

	Light curve-based Model	Spectroscopy-based Model	Combined Model
General Input	Galactic coordinate, Parallax, Gaia magnitude		
Specific Input	ρ_*	T_{eff} , [Fe/H]	T_{eff} , [Fe/H], ρ_*

NOTE—In the stellar modeling with **BASTA**, the unit of stellar density is g/cm^3 .

As described in the `juliet` documentation, the fitted parameters can be grouped into two categories. The first category includes planetary parameters: the orbital period, epoch time, impact parameter, planet-to-star radius ratio, and stellar density. The prior hyperparameters for the orbital period and epoch time were informed by results from the BLS periodogram generated using `lightkurve`. The prior for stellar density was set to span 0.1–15.0 g/cm^{-3} , a range that encompasses the stellar densities of the sample stars in this study. For the impact parameter and the planet-to-star radius ratio, rather than fitting them directly, we adopted a joint sampling approach based on the method proposed by N. Espinoza (2018). This method samples two intermediate variables from uniform distributions bounded between 0 and 1, ensuring that the resulting values of the impact parameter and the planet-to-star radius ratio are physically meaningful for a transit event. In particular, this prevents the sampling of configurations where the combination of planet-to-star radius ratio and impact parameter would result in a non-transiting geometry, as defined in Equation 1. The second category comprises instrument-related parameters, including the limb-darkening coefficients, dilution factor, flux offset, and jitter term. For these parameters, we adopted the default priors recommended in the `juliet` documentation for TESS data. Specifically, the limb-darkening coefficients follow the reparameterization scheme introduced by D. M. Kipping (2013) for the quadratic two-coefficient limb-darkening law.

Using the approach described above, we performed transit fitting for all 100 exoplanet systems in our sample. The results are presented in Section 4.1.

3.2. Stellar Modeling

Stellar modeling was conducted using **BASTA**, a grid-based Bayesian inference tool that compares observed stellar parameters against pre-computed evolutionary tracks. In this study, we adopted the BaSTI stellar evolution grid (S. L. Hidalgo et al. 2018) to estimate the mass, radius, and age of each host star in our sample. To assess the impact of transit-derived constraints on stellar characterization, we applied three modeling configurations to each star: a light curve-based model, a spectroscopy-based model, and a combined model. The input parameters used in each model are listed in Table 2. All models included the same set of general inputs, galactic coordinates, parallax, and Gaia magnitude. These inputs help improve modeling precision and support the convergence of the posterior distributions. For the model-specific inputs, the light curve-based model included only the stellar density derived from transit fitting. The spectroscopy-based model used the effective temperature and metallicity obtained from existing spectroscopic observations. The combined model incorporated all of the above parameters.

When using the **BASTA** code³ in combination with the BaSTI isochrones, it is necessary to

³ <https://github.com/BASTAcode/BASTA>

Table 3. Transit Fitting Results

Planet Name	ρ_* (g/cm ³)	$\frac{R_p}{R_*}$	b
HAT-P-69b	$0.371^{+0.031}_{-0.024}$	$0.08405^{+0.00047}_{-0.00057}$	$0.286^{+0.067}_{-0.122}$
HATS-6b	$4.758^{+0.481}_{-0.515}$	$0.16802^{+0.00397}_{-0.00407}$	$0.318^{+0.107}_{-0.176}$
HATS-71b	$6.180^{+0.487}_{-0.428}$	$0.21520^{+0.00284}_{-0.00418}$	$0.363^{+0.059}_{-0.098}$
NGTS-24b	$1.257^{+0.558}_{-0.665}$	$0.06392^{+0.00474}_{-0.00310}$	$0.511^{+0.245}_{-0.282}$
TOI-674b	$9.828^{+1.243}_{-1.051}$	$0.11276^{+0.00199}_{-0.00215}$	$0.628^{+0.045}_{-0.052}$
TOI-1075b	$0.778^{+0.411}_{-0.427}$	$0.02109^{+0.00298}_{-0.00207}$	$0.431^{+0.359}_{-0.309}$
TOI-1416b	$1.245^{+0.708}_{-0.498}$	$0.01949^{+0.00156}_{-0.00102}$	$0.651^{+0.131}_{-0.169}$
TOI-1759b	$1.688^{+0.636}_{-0.443}$	$0.05168^{+0.00137}_{-0.00115}$	$0.672^{+0.072}_{-0.106}$
TOI-2136b	$12.516^{+1.900}_{-3.534}$	$0.05539^{+0.00222}_{-0.00244}$	$0.430^{+0.170}_{-0.192}$
TOI-2977b	$1.107^{+0.042}_{-0.057}$	$0.10536^{+0.00095}_{-0.00104}$	$0.105^{+0.116}_{-0.070}$
WASP-17b	$0.504^{+0.033}_{-0.028}$	$0.12148^{+0.00097}_{-0.00115}$	$0.297^{+0.061}_{-0.098}$
WASP-121b	$0.643^{+0.008}_{-0.011}$	$0.12097^{+0.00028}_{-0.00021}$	$0.110^{+0.050}_{-0.068}$
WASP-174b	$0.623^{+0.178}_{-0.087}$	$0.43867^{+0.33563}_{-0.22427}$	$1.326^{+0.349}_{-0.238}$
WASP-178b	$0.551^{+0.021}_{-0.019}$	$0.10773^{+0.00044}_{-0.00060}$	$0.580^{+0.015}_{-0.018}$
WASP-187b	$0.110^{+0.012}_{-0.007}$	$0.05994^{+0.00047}_{-0.00041}$	$0.728^{+0.014}_{-0.024}$

NOTE—Results from transit fitting for the 15 selected samples, including the special cases discussed in the text and other well-performed samples. Results for the full set of 100 samples are available in the machine-readable table (MRT). Stellar density values in the MRT are given in units of kg/m³.

specify the appropriate physical model according to the properties of each host star. Based on the physical considerations discussed in A. Pietrinferni et al. (2004), we adopted a stellar mass threshold of $1.15M_\odot$, enabling convective core overshooting for stars more massive than this limit, and including atomic diffusion for lower-mass stars.

Using the approach described above, we performed stellar modeling for all 100 host stars in our sample. The results are presented in Section 4.2

4. RESULTS

4.1. Transit Fitting Results

Based on the methods described in Section 3.1, we performed Bayesian transit fitting for 100 transiting exoplanet systems. The fitting parameters of particular interest were stellar density, planet-to-star radius ratio, and impact parameter. Results for 15 representative systems selected from the full sample are pre-

sented in Table 3; the complete results for all 100 systems are provided in the accompanying machine-readable table (MRT). Stellar density was subsequently used as an input parameter for stellar modeling in Section 4.2, while the planet-to-star radius ratio and impact parameter were employed to characterize transit morphology and compared against existing values from the NASA Exoplanet Archive. According to the criteria defined in Section 2, 87 systems were categorized into the 'ideal' group, 10 systems into the 'small radius ratio' group, and the remaining 3 systems into the 'V-shaped' group.

As shown in Figure 2, we present comparisons of the fitted stellar densities and planet-to-star radius ratios from this study against values reported in the NASA Exoplanet Archive for the three defined sample groups. According to Equation 4, the mean absolute relative residuals in the planet-to-star radius ratio for the 'ideal', 'V-shaped', and 'small radius ratio' groups are 0.03011, 2.56815, and 0.07655, respectively. For stellar density, the corresponding mean absolute relative residuals are 0.14383, 0.36573, and 0.26647, respectively.

$$r_{\text{rel}} = \frac{|x_{\text{arch}} - x_{\text{fit}}|}{x_{\text{arch}}} \quad (4)$$

Due to the large residuals present in some results from the 'V-shaped' and 'small radius ratio' groups, the scales in Figure 2 were expanded, causing certain details to be obscured. To clearly illustrate these finer details, Figure 3 shows the comparison of fitted and archived values for stellar density and planet-to-star radius ratio, restricted exclusively to the 'ideal' group.

4.2. Stellar Modeling Results

Based on the methods described in Section 3.2, we performed Bayesian stellar modeling for 100 host stars using the BaSTI stellar evolution grid (S. L. Hidalgo et al. 2018). For each star, three models were applied: a light curve-based model, a spectroscopy-based

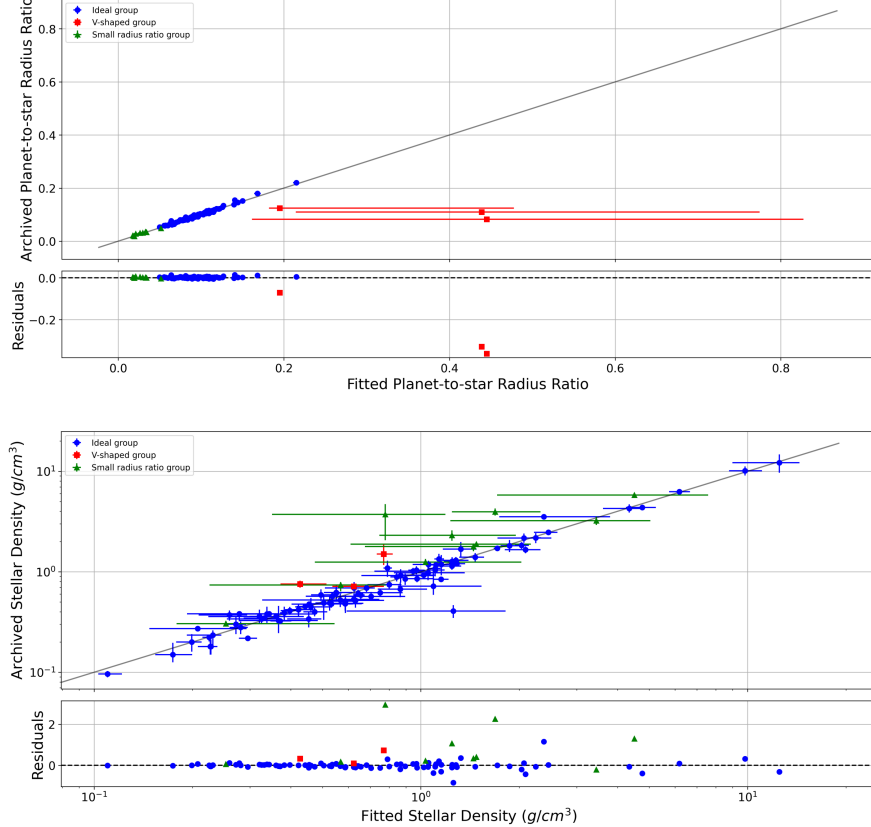


Figure 2. Comparison between fitted and archived values of the planet-to-star radius ratio and stellar density, along with the corresponding residuals, for all three groups.

model, and a combined model. The key output parameters of interest were stellar mass, stellar radius, and stellar age. Tables 4–6 present the stellar modeling results from three models for the 15 representative host stars corresponding to the systems listed in Table 3. The full modeling results for all 100 systems are available in the accompanying MRT. Figure 4 shows the posterior distributions of the output parameters from the three models, using WASP-17 as an illustrative example.

Based on the stellar masses and radii derived from the combined model, the host stars in our sample span all main-sequence spectral types except the most massive O-type stars. TOI-2136 has the smallest mass and radius, $0.303 M_{\odot}$ and $0.306 R_{\odot}$, respectively, while WASP-178 has the largest mass, $2.189 M_{\odot}$, and WASP-187 has the largest radius, $2.748 R_{\odot}$.

To more clearly compare the performance of the three stellar modeling approaches, Figure 5 shows the relative uncertainties in stellar mass, radius, and age, as defined in Equation 5, across all 100 host stars. The lower and upper uncertainties correspond to the 16th and 84th percentiles of the posterior distributions, respectively.

$$\Delta_{\text{rel}} = \frac{1}{2} \cdot \frac{\Delta_+ + \Delta_-}{x_{\text{median}}} \quad (5)$$

One notable outlier, HATS-6, was identified in the stellar age estimates produced by the spectroscopy-based model. As shown in Table 5, it exhibited an unusually young age with a large upper uncertainty, resulting in a relative age uncertainty of 42.7. To prevent this single case from skewing the overall distribution, HATS-6 was excluded from the stellar age his-

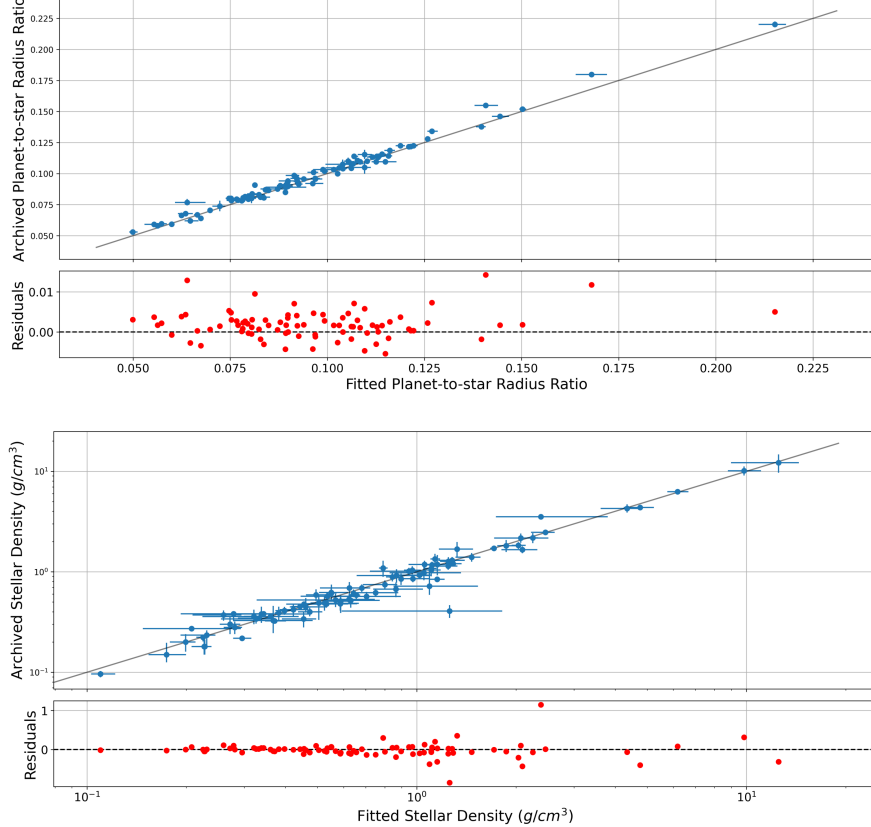


Figure 3. Comparison between fitted and archived values of the planet-to-star radius ratio and stellar density, along with the corresponding residuals, for the ‘ideal’ group only.

togram in Figure 5 and subsequent statistical analyses.

Based on Equation 5, we also computed the mean relative uncertainties of the stellar parameters across the host stars under each modeling approach. For stellar mass, the mean relative uncertainties were 0.16984 for the light curve-based model, 0.04442 for the spectroscopy-based model, and 0.04082 for the combined model. For stellar radius, the corresponding values were 0.07454, 0.05942, and 0.03217. For stellar age, the mean relative uncertainties were 0.71064, 0.35904, and 0.28925, respectively.

Overall, the stellar parameter estimates obtained from the three modeling approaches are broadly consistent. However, a few systems exhibit noticeable discrepancies. For example, TOI-1075 and TOI-1759 yield exception-

ally young stellar ages of only 0.02 Gyr under the light curve-based model, which contrasts sharply with the spectroscopy-based estimates of 11.00 Gyr and 10.20 Gyr, respectively. Conversely, HATS-6 and HATS-71 shows an unusually young age of 0.05 Gyr and 0.04 Gyr under the spectroscopy-based model, compared to 10.20 Gyr and 3.5 Gyr from the light curve-based model, respectively. In all four cases, the combined model results appear to be influenced by the outlying estimates, yielding final ages close to the anomalously young values.

5. DISCUSSION

In the transit fitting results, distinct patterns emerged across different groups, as illustrated in Figure 2. The ‘ideal’ group exhibited the smallest relative residuals in both the planet-to-star radius ratio and stellar density, which aligns

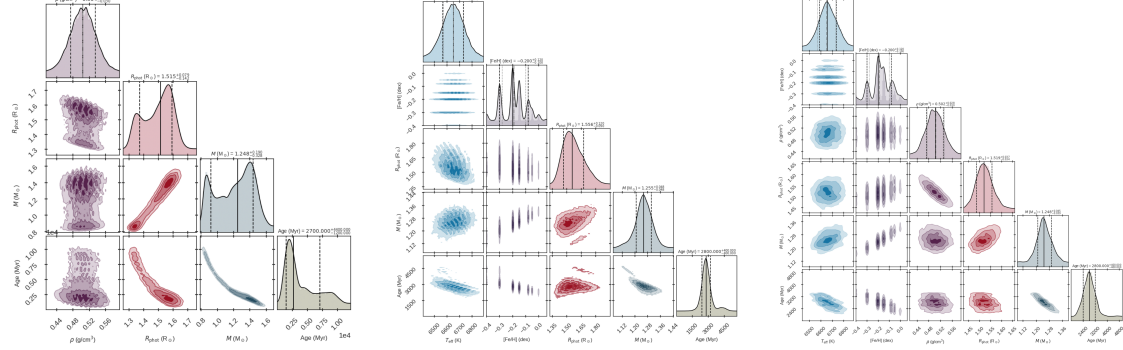


Figure 4. Example posterior distributions from stellar modeling for WASP-17. The left panel shows results from the light curve–based model, the center panel from the spectroscopy-based model, and the right panel from the combined model.

Table 4. Light Curve-based Model Results

Star Name	M_* (M_\odot)	R_* (R_\odot)	Age (Gyr)
HATS-P-69	$1.572^{+0.241}_{-0.393}$	$1.812^{+0.099}_{-0.161}$	$1.30^{+1.80}_{-0.60}$
HATS-6	$0.584^{+0.050}_{-0.025}$	$0.557^{+0.024}_{-0.022}$	$10.20^{+6.20}_{-6.60}$
HATS-71	$0.492^{+0.019}_{-0.261}$	$0.458^{+0.011}_{-0.080}$	$3.50^{+10.50}_{-3.47}$
NGTS-24	$1.043^{+0.147}_{-0.143}$	$1.098^{+0.253}_{-0.140}$	$3.40^{+4.00}_{-2.40}$
TOI-674	$0.420^{+0.025}_{-0.028}$	$0.396^{+0.022}_{-0.025}$	$10.60^{+6.30}_{-7.20}$
TO-1075	$0.612^{+0.018}_{-0.049}$	$0.801^{+0.010}_{-0.048}$	$0.02^{+0.00}_{-0.00}$
TOI-1416	$0.786^{+0.053}_{-0.058}$	$0.788^{+0.027}_{-0.040}$	$12.60^{+5.10}_{-6.40}$
TOI-1759	$0.584^{+0.066}_{-0.060}$	$0.734^{+0.077}_{-0.057}$	$0.02^{+0.01}_{-0.00}$
TOI-2136	$0.339^{+0.024}_{-0.028}$	$0.334^{+0.021}_{-0.023}$	$10.40^{+6.20}_{-6.90}$
TOI-2977	$1.026^{+0.136}_{-0.132}$	$1.093^{+0.051}_{-0.052}$	$3.10^{+2.80}_{-2.00}$
WASP-17	$1.248^{+0.190}_{-0.328}$	$1.515^{+0.079}_{-0.142}$	$2.70^{+4.40}_{-1.20}$
WASP-121	$1.313^{+0.225}_{-0.343}$	$1.422^{+0.077}_{-0.135}$	$1.70^{+4.00}_{-1.30}$
WASP-174	$1.147^{+0.205}_{-0.280}$	$1.373^{+0.114}_{-0.126}$	$3.60^{+5.00}_{-2.10}$
WASP-178	$1.936^{+0.261}_{-0.301}$	$1.704^{+0.076}_{-0.090}$	$0.55^{+0.55}_{-0.41}$
WASP-187	$1.609^{+0.122}_{-0.483}$	$2.701^{+0.127}_{-0.258}$	$2.20^{+1.70}_{-0.40}$

NOTE—Stellar modeling results from the light curve–based model for the same sample as in Table 3. Results for the complete sample of 100 host stars are available in the machine-readable table.

Table 5. Spectroscopy-based Model Results

Star Name	M_* (M_\odot)	R_* (R_\odot)	Age (Gyr)
HATS-P-69	$1.639^{+0.061}_{-0.059}$	$1.985^{+0.339}_{-0.249}$	$1.30^{+0.40}_{-0.45}$
HATS-6	$0.619^{+0.034}_{-0.046}$	$0.630^{+0.054}_{-0.069}$	$0.05^{+4.25}_{-0.02}$
HATS-71	$0.300^{+0.010}_{-0.008}$	$0.445^{+0.028}_{-0.028}$	$0.04^{+0.01}_{-0.01}$
NGTS-24	$1.170^{+0.099}_{-0.044}$	$1.637^{+0.074}_{-0.070}$	$6.80^{+0.90}_{-2.00}$
TOI-674	$0.437^{+0.035}_{-0.019}$	$0.412^{+0.023}_{-0.017}$	$10.00^{+6.30}_{-6.40}$
TO-1075	$0.569^{+0.025}_{-0.018}$	$0.545^{+0.024}_{-0.018}$	$11.00^{+6.10}_{-7.80}$
TOI-1416	$0.801^{+0.026}_{-0.024}$	$0.783^{+0.022}_{-0.020}$	$11.30^{+5.90}_{-6.40}$
TOI-1759	$0.631^{+0.020}_{-0.021}$	$0.607^{+0.015}_{-0.016}$	$10.20^{+6.40}_{-6.60}$
TOI-2136	$0.323^{+0.015}_{-0.016}$	$0.320^{+0.012}_{-0.012}$	$10.60^{+6.40}_{-7.00}$
TOI-2977	$1.013^{+0.036}_{-0.034}$	$1.367^{+0.086}_{-0.078}$	$10.00^{+1.50}_{-1.80}$
WASP-17	$1.255^{+0.048}_{-0.048}$	$1.556^{+0.120}_{-0.090}$	$2.80^{+0.40}_{-0.40}$
WASP-121	$1.446^{+0.042}_{-0.044}$	$1.813^{+0.113}_{-0.102}$	$2.20^{+0.30}_{-0.40}$
WASP-174	$1.270^{+0.034}_{-0.037}$	$1.494^{+0.087}_{-0.106}$	$3.00^{+0.40}_{-0.50}$
WASP-178	$2.193^{+0.081}_{-0.089}$	$1.847^{+0.113}_{-0.083}$	$0.20^{+0.14}_{-0.11}$
WASP-187	$1.577^{+0.069}_{-0.088}$	$2.682^{+0.182}_{-0.140}$	$2.30^{+0.30}_{-0.30}$

NOTE—Stellar modeling results from the spectroscopy–based model for the same sample as in Table 3. Results for the complete sample of 100 host stars are available in the machine-readable table.

with expectations. In contrast, the ‘V-shaped’ group showed overestimated planet-to-star radius ratios with large uncertainties, suggesting that the adopted transit model may not adequately handle the geometry of V-shaped light curves. For the ‘small radius ratio’ group, the fitted planet-to-star radius ratios agreed well with reported values from the NASA Exoplanet Archive, but the fitted stellar densities were sys-

tematically underestimated. According to S. Seager & G. Mallen-Ornelas (2003), stellar density depends on several transit parameters, including orbital period, transit depth, impact parameter, and total transit duration. We suggest that the low signal-to-noise ratios in this group hindered the precise identification of transit boundaries, leading to inaccurate estimates

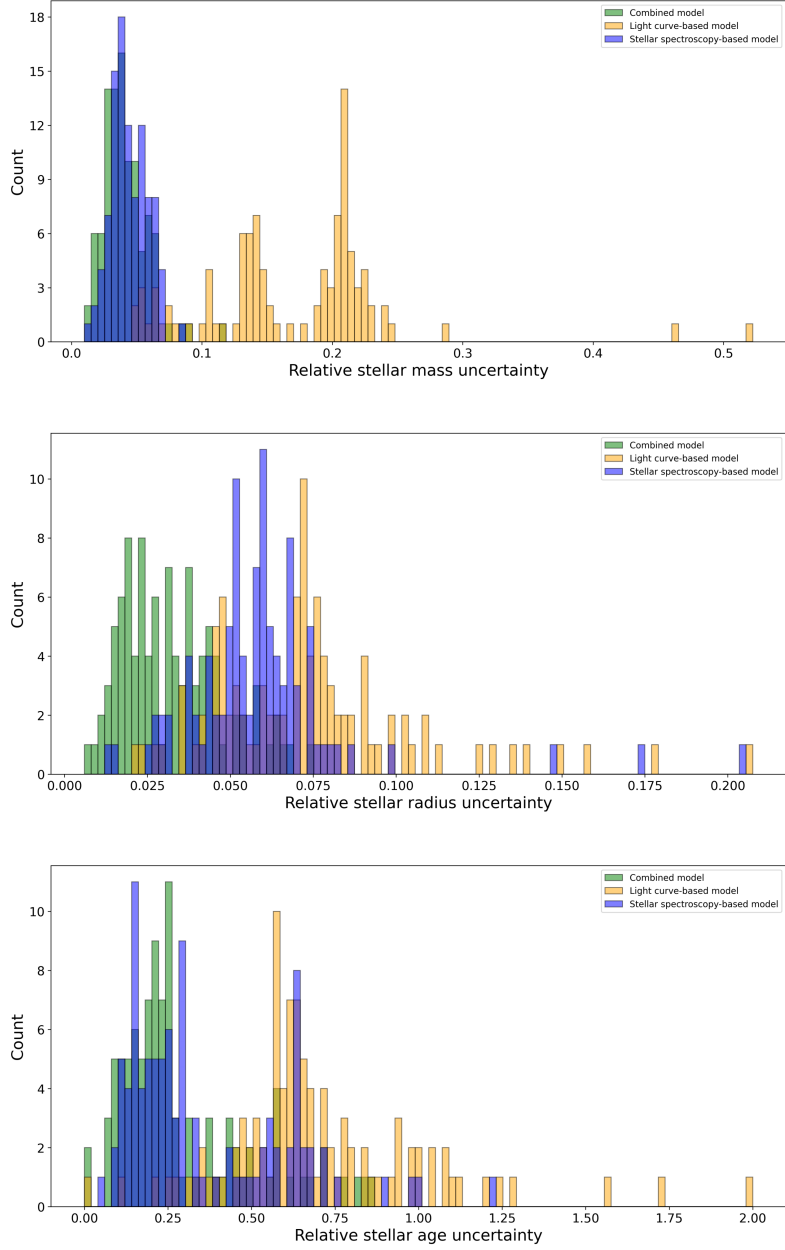


Figure 5. Comparison of relative uncertainties in stellar mass, radius, and age obtained from the light curve–based model, spectroscopy-based model, and the combined model.

of total transit time and, consequently, stellar density.

From the stellar modeling results shown in Figure 5, the combined model provides the largest gain in stellar radius precision, achieving a mean relative uncertainty of approximately 3.2% in this study. For stellar mass, both the combined and spectroscopy-based models

yield substantially tighter constraints than the light curve–based model, with the combined model reaching a precision of about 4.1%, indicating that stellar density alone provides relatively weak constraints on stellar mass. In the case of stellar age, all three models deliver comparatively weak constraints; even the combined model attains an average precision of only

Table 6. Combined Model Results

Star Name	M_* (M_\odot)	R_* (R_\odot)	Age (Gyr)
HATS-P-69	$1.690^{+0.048}_{-0.068}$	$1.862^{+0.046}_{-0.049}$	$1.00^{+0.20}_{-0.10}$
HATS-6	$0.619^{+0.014}_{-0.059}$	$0.593^{+0.025}_{-0.028}$	$0.06^{+0.02}_{-0.01}$
HATS-71	$0.305^{+0.005}_{-0.005}$	$0.417^{+0.007}_{-0.007}$	$0.05^{+0.00}_{-0.00}$
NGTS-24	$1.173^{+0.098}_{-0.046}$	$1.629^{+0.075}_{-0.069}$	$6.70^{+1.00}_{-1.90}$
TOI-674	$0.429^{+0.021}_{-0.025}$	$0.405^{+0.017}_{-0.013}$	$9.90^{+6.70}_{-6.30}$
TOI-1075	$0.563^{+0.016}_{-0.016}$	$0.754^{+0.010}_{-0.010}$	$0.02^{+0.00}_{-0.00}$
TOI-1416	$0.788^{+0.028}_{-0.016}$	$0.796^{+0.016}_{-0.021}$	$15.50^{+3.10}_{-6.60}$
TOI-1759	$0.604^{+0.045}_{-0.095}$	$0.655^{+0.024}_{-0.019}$	$0.03^{+0.02}_{-0.01}$
TOI-2136	$0.303^{+0.013}_{-0.013}$	$0.306^{+0.010}_{-0.010}$	$11.60^{+5.90}_{-7.00}$
TOI-2977	$1.076^{+0.019}_{-0.036}$	$1.128^{+0.016}_{-0.017}$	$4.50^{+1.10}_{-0.70}$
WASP-17	$1.248^{+0.045}_{-0.039}$	$1.519^{+0.037}_{-0.034}$	$2.80^{+0.40}_{-0.40}$
WASP-121	$1.527^{+0.011}_{-0.019}$	$1.499^{+0.007}_{-0.011}$	$0.32^{+0.14}_{-0.10}$
WASP-174	$1.266^{+0.034}_{-0.036}$	$1.468^{+0.076}_{-0.080}$	$2.90^{+0.40}_{-0.40}$
WASP-178	$2.189^{+0.062}_{-0.082}$	$1.778^{+0.028}_{-0.029}$	$0.12^{+0.10}_{-0.07}$
WASP-187	$1.615^{+0.045}_{-0.050}$	$2.748^{+0.071}_{-0.076}$	$2.10^{+0.20}_{-0.10}$

NOTE—Stellar modeling results from the combined model for the same sample as in Table 3. Results for the complete sample of 100 host stars are available in the machine-readable table.

28.9%. This result is consistent with the findings of N. Gai et al. (2011), who reported that stellar age estimates are highly dependent on the adopted stellar model grid and are subject to substantially larger uncertainties.

Beyond these general trends, several individual systems display noteworthy deviations. TOI-1075 and TOI-1759 yield anomalously young stellar ages in the light curve-based model, likely due to inaccurate stellar density estimates in the transit fitting stage caused by their small planet-to-star radius ratios. In contrast, HATS-6 and HATS-71 exhibit anomalously young ages in the spectroscopy-based model. Since the input parameters for this model are drawn entirely from the NASA Exoplanet Archive, the origin of these discrepancies remains unclear.

A limitation of this study is that it considers only transiting exoplanets in single-star, single-planet systems with circular orbits, which represent only a small fraction of all known exoplanets. However, the pipeline developed for

this work is capable of incorporating orbital eccentricity and multi-planet transits during the fitting stage. This can be achieved in practice by including the corresponding additional parameters when performing the transit fits with `juliet`. Future studies could take advantage of this capability to analyze a substantially larger sample. Another limitation is that the stellar modeling stage employed only the BaSTI stellar grid. As noted by N. Gai et al. (2011), stellar age estimates are often highly sensitive to the choice of stellar model grid. Building on the present work, future analyses could use `BASTA` to incorporate other stellar grids, compare the resulting parameter estimates, and evaluate differences between grids. Finally, the four anomalous cases identified in the stellar modeling results should be investigated in greater detail in future work to determine the causes of these deviations.

6. CONCLUSION

In this study, we performed transit light-curve fitting and stellar modeling for 100 transiting exoplanet systems using a Bayesian inference framework. The sample consisted exclusively of single-star, single-planet systems with known circular orbits, and the host stars spanned spectral types from the smallest M type up to B type. Using TESS photometric data, we derived planetary parameters including orbital period, epoch time, planet-to-star radius ratio, and impact parameter, as well as stellar density for each host star. For the majority of systems, classified as the 'ideal' group, the fitted planet-to-star radius ratios and stellar densities show overall good agreement with the values reported in the NASA Exoplanet Archive, with mean absolute relative residuals of 3.0% for the planet-to-star radius ratio and 14.4% for stellar density. In contrast, a small subset of systems with V-shaped light curves or with planet-to-star radius ratios below 0.05 exhibits a higher incidence of discrepancies, consistent with the greater diffi-

culty of obtaining precise parameter estimates in such configurations.

We applied three modeling approaches—the light curve-based model, the spectroscopy-based model, and the combined model—to estimate the masses, radii, and ages of 100 host stars. For the vast majority of systems, the results from the three models are consistent with one another. Among them, the combined model provides the tightest constraints on all three parameters, with mean relative uncertainties of 4.1%, 3.2%, and 28.9% for stellar mass, radius, and age, respectively, based on the 68% credible interval. However, a few individual systems show substantial discrepancies in the stellar ages derived from different models, and the underlying causes remain unclear.

These results provide robust planetary and stellar parameters for the analyzed exoplanet systems, enabling a more complete characterization of their properties. In particular, our analysis offers supplementary constraints for planets whose impact parameters have been previously unavailable or only weakly constrained. Likewise, for host stars that were previously modeled solely through spectroscopy, our transit fitting provides an additional reliable input parameter—the stellar density—thereby enhancing the characterization of their fundamental physical properties. The methodology developed in this work can be extended in future applications to multi-planet and non-circular orbit transit systems, substantially increasing the potential sample size. In addition, employing multiple stellar evolution grids for host-star modeling could improve the precision and robustness

of parameter estimates by reducing the dependence on any single grid.

ACKNOWLEDGMENTS

I would like to express my sincere gratitude to Dr. Vincent Van Eylen for his supervision and support throughout this project. I am also grateful to Dr. Angharad Weeks and Dr. Edward Bryant for their helpful discussions and valuable advice during the research process.

This paper includes data collected with the TESS mission, obtained from the MAST data archive at the Space Telescope Science Institute (STScI). Funding for the TESS mission is provided by the NASA Explorer Program. STScI is operated by the Association of Universities for Research in Astronomy, Inc., under NASA contract NAS 5-2655.

This research has made use of the NASA Exoplanet Archive, which is operated by the California Institute of Technology, under contract with the National Aeronautics and Space Administration under the Exoplanet Exploration Program.

Software: `lightkurve` ([Lightkurve Collaboration et al. 2018](#)), `astroquery` ([A. Ginsburg et al. 2019](#)), `astropy` ([Astropy Collaboration et al. 2022](#)), `juliet` ([N. Espinoza et al. 2019](#)), `batman` ([L. Kreidberg 2015](#)), `dynesty` ([J. S. Speagle 2020](#)), `corner.py` ([D. Foreman-Mackey 2016](#)), `BASTA` ([V. Silva Aguirre et al. 2015; V. Aguirre Børnsen-Koch et al. 2021](#)), `NumPy` ([C. R. Harris et al. 2020](#)), `SciPy` ([P. Virtanen et al. 2020](#)), `Matplotlib` ([J. D. Hunter 2007](#))

REFERENCES

- Aguirre Børnsen-Koch, V., Rørsted, J. L., Justesen, A. B., et al. 2021, Monthly Notices of the Royal Astronomical Society, 509, 4344–4364,
doi: [10.1093/mnras/stab2911](https://doi.org/10.1093/mnras/stab2911)

- Astropy Collaboration, Price-Whelan, A. M., Lim, P. L., et al. 2022, ApJ, 935, 167,
doi: [10.3847/1538-4357/ac7c74](https://doi.org/10.3847/1538-4357/ac7c74)

- Borucki, W. J., Koch, D., Basri, G., et al. 2010, *Science*, 327, 977–980, doi: [10.1126/science.1185402](https://doi.org/10.1126/science.1185402)
- Espinoza, N. 2018, *Research Notes of the American Astronomical Society*, 2, 209, doi: [10.3847/2515-5172/aaef38](https://doi.org/10.3847/2515-5172/aaef38)
- Espinoza, N., Kossakowski, D., & Brahm, R. 2019, *MNRAS*, 490, 2262, doi: [10.1093/mnras/stz2688](https://doi.org/10.1093/mnras/stz2688)
- Foreman-Mackey, D. 2016, *The Journal of Open Source Software*, 1, 24, doi: [10.21105/joss.00024](https://doi.org/10.21105/joss.00024)
- Gai, N., Basu, S., Chaplin, W. J., & Elsworth, Y. 2011, *The Astrophysical Journal*, 730, 63, doi: [10.1088/0004-637x/730/2/63](https://doi.org/10.1088/0004-637x/730/2/63)
- Ginsburg, A., Sipőcz, B. M., Brasseur, C. E., et al. 2019, *The Astronomical Journal*, 157, 98, doi: [10.3847/1538-3881/aafc33](https://doi.org/10.3847/1538-3881/aafc33)
- Harris, C. R., Millman, K. J., van der Walt, S. J., et al. 2020, *Nature*, 585, 357–362, doi: [10.1038/s41586-020-2649-2](https://doi.org/10.1038/s41586-020-2649-2)
- Hidalgo, S. L., Pietrinferni, A., Cassisi, S., et al. 2018, *The Astrophysical Journal*, 856, 125, doi: [10.3847/1538-4357/aab158](https://doi.org/10.3847/1538-4357/aab158)
- Hunter, J. D. 2007, *Computing in Science & Engineering*, 9, 90, doi: [10.1109/MCSE.2007.55](https://doi.org/10.1109/MCSE.2007.55)
- Jenkins, J. M., Twicken, J. D., McCauliff, S., et al. 2016, in *Software and Cyberinfrastructure for Astronomy IV*, ed. G. Chiozzi & J. C. Guzman, Vol. 9913 (SPIE), 99133E, doi: [10.1117/12.2233418](https://doi.org/10.1117/12.2233418)
- Kipping, D. M. 2013, *Monthly Notices of the Royal Astronomical Society*, 435, 2152, doi: [10.1093/mnras/stt1435](https://doi.org/10.1093/mnras/stt1435)
- Kreidberg, L. 2015, *Publications of the Astronomical Society of the Pacific*, 127, 1161–1165, doi: [10.1086/683602](https://doi.org/10.1086/683602)
- Lightkurve Collaboration, Cardoso, J. V. d. M., Hedges, C., et al. 2018, Lightkurve: Kepler and TESS time series analysis in Python,, *Astrophysics Source Code Library*, record ascl:1812.013
- Mayor, M., & Queloz, D. 1995, *Nature*, 378, 355–359, doi: [10.1038/378355a0](https://doi.org/10.1038/378355a0)
- NASA Exoplanet Archive. 2020, *Planetary Systems*, NExSci-Caltech/IPAC, doi: [10.26133/NEA12](https://doi.org/10.26133/NEA12)
- NASA Exoplanet Archive. 2024, *Stellar Parameters for Planetary Hosts Table*, NExSci-Caltech/IPAC, doi: [10.26133/NEA40](https://doi.org/10.26133/NEA40)
- Pietrinferni, A., Cassisi, S., Salaris, M., & Castelli, F. 2004, *The Astrophysical Journal*, 612, 168–190, doi: [10.1086/422498](https://doi.org/10.1086/422498)
- Prusti, T., de Bruijne, J. H. J., Brown, A. G. A., et al. 2016, *Astronomy and Astrophysics*, 595, A1, doi: [10.1051/0004-6361/201629272](https://doi.org/10.1051/0004-6361/201629272)
- Ricker, G. R., Winn, J. N., Vanderspek, R., et al. 2014, in *Space Telescopes and Instrumentation 2014: Optical, Infrared, and Millimeter Wave*, ed. J. M. Oschmann, M. Clampin, G. G. Fazio, & H. A. MacEwen, Vol. 9143 (SPIE), 914320, doi: [10.1117/12.2063489](https://doi.org/10.1117/12.2063489)
- Sandford, E., & Kipping, D. 2017, *The Astronomical Journal*, 154, 228, doi: [10.3847/1538-3881/aa94bf](https://doi.org/10.3847/1538-3881/aa94bf)
- Savitzky, A., & Golay, M. J. E. 1964, *Analytical Chemistry*, 36, 1627–1639, doi: [10.1021/ac60214a047](https://doi.org/10.1021/ac60214a047)
- Seager, S., & Mallen-Ornelas, G. 2003, *The Astrophysical Journal*, 585, 1038–1055, doi: [10.1086/346105](https://doi.org/10.1086/346105)
- Silva Aguirre, V., Davies, G. R., Basu, S., et al. 2015, *Monthly Notices of the Royal Astronomical Society*, 452, 2127–2148, doi: [10.1093/mnras/stv1388](https://doi.org/10.1093/mnras/stv1388)
- Speagle, J. S. 2020, *MNRAS*, 493, 3132, doi: [10.1093/mnras/staa278](https://doi.org/10.1093/mnras/staa278)
- Takeda, G., Ford, E. B., Sills, A., et al. 2007, *The Astrophysical Journal Supplement Series*, 168, 297–318, doi: [10.1086/509763](https://doi.org/10.1086/509763)
- Torres, G., Fischer, D. A., Sozzetti, A., et al. 2012, *The Astrophysical Journal*, 757, 161, doi: [10.1088/0004-637x/757/2/161](https://doi.org/10.1088/0004-637x/757/2/161)
- Virtanen, P., Gommers, R., Oliphant, T. E., et al. 2020, *Nature Methods*, 17, 261–272, doi: [10.1038/s41592-019-0686-2](https://doi.org/10.1038/s41592-019-0686-2)